Fermi National Accelerator Laboratory

FERMILAB-Pub-97/242-E
DØ

Fixed Cone Jet Definitions in DØ and R_{sep}.

B. Abbott et al.

Fermi National Accelerator Laboratory
P.O. Box 500, Batavia, Illinois 60510

September 1997

Operated by Universities Research Association Inc. under Contract No. DE-AC02-76CH03000 with the United States Department of Energy

Disclaimer

Distribution

Fermilab-PUB-97/242-E

Fixed Cone Jet Definitions in DØ and R_{sep}.

B. Abbott[1], M. Bhattacharjee[2], D. Elvira[3], F. Nang[4], H. Weerts[5]

August 7, 1997

[1] *New York University, New York, New York 10003*
[2] *Delhi University, Delhi, India 110077*
[3] *Fermi National Accelerator Laboratory, Batavia, Illinois 60510*
[4] *Brown University, Providence, Rhode Island 02912*
[5] *Michigan State University, East Lansing, Michigan 48824*

Abstract

This document describes the status and usage of the DØ fixed cone jet algorithm. The note begins with a status report on cone algorithms as used by DØ for QCD comparisons. The second section describes how the phenomenological parameter R_{sep} was determined from experimental data. R_{sep} is the maximum distance divided by the fixed jet cone size allowed between two partons. If the parton distance is less than R_{sep}, jets are merged using the Snowmass jet algorithm. R_{sep} was determined by overlaying two experimental jets and determining the jet distances at which the two jets were identified as one jet by the experimental splitting/merging algorithm. The value of R_{sep} was also determined by parameterizing the jet shapes measured in DØ as a function of the jet transverse energy and determining analytically the jet distance at which two jets are identified as one jet. We conclude that the value $R_{sep} = 1.3$ reflects the DØ merging/splitting criteria the best. We adopt this value as the standard to be used in all NLO theoretical predictions using the Snowmass jet algorithm. The jet inclusive cross section has been calculated in next-to-leading perturbative QCD as a function of R_{sep}. The variation in the theoretical prediction is presented in the last section of the document.

Contents

1 Introduction

For QCD comparisons, quantitative jet analyses depend on the definition of a jet both experimentally and theoretically. For the purpose of this document, theory refers to next-to-leading (NLO) perturbative calculations and experiment refers to calorimeter level jet reconstruction. At the NLO parton level, the jet can consist of at most two partons, whereas in the experiment a jet consists of the energy deposits of particles in the calorimeter. Traditionally, a jet is defined with a fixed cone size which is defined in η, ϕ space where ϕ is the azimuthal angle, $\eta = -\ln(\tan\theta/2)$ is the pseudorapidity and θ is the angle with respect to the beam. The cone size is defined as $R = \sqrt{\Delta^2\phi + \Delta^2\eta}$, where $\Delta\phi, \Delta\eta$ are the distances in η, ϕ space. Typically the cone is chosen as $R = 0.7$ for several reasons:

- A cone of size 0.7 empirically contains most of the energy of a jet and has the best jet energy resolution.
- NLO order predictions are most stable and do not depend strongly on renormalization and factorization scale at this cone size. [1]
- It is a standard size used by many experiments at present energies.

This document begins by describing the jet clustering algorithm used in NLO theoretical calculations. Next, it describes the jet clustering algorithm used by DØ. Because the jet clustering algorithm at NLO and DØ differ in their treatment of overlapping jets, quantitative comparisons to theoretical predictions are difficult. We therefore use a parameter, R_{sep}, which limits the maximum distance allowed between two partons at NLO. The value of R_{sep} depends upon the experimental treatment of overlapping jets, so we have measured R_{sep} for the DØ jet clustering algorithm. Two different techniques to obtain R_{sep} are presented as a function of jet E_T, η and cone size. The note concludes with the effects of different choices of R_{sep} on the jet inclusive cross section and a recommendation for the R_{sep} value which should be used when comparing NLO theoretical predictions to DØ data.

2 Jet definitions

Intuitively the use of a fixed cone is rather simple and straightforward. The same cone size is applied at the theory and experimental level. However, in practice it is impossible to apply *exactly* the same algorithm at NLO and at the calorimeter level. Some of these differences are simply conventions, while others are caused by experimental procedures. In the next sections we will describe the jet definitions used by both theory and the DØ experiment.

2.1 Jets at NLO QCD and the Snowmass Accord

To make the application of the jet clustering algorithm more uniform, several theorists and experimentalists agreed on the so called Snowmass Accord [2]. This accord specifies which partons should be clustered to form a jet at the theory level. The accord does not give clear instructions for the treatment of jets experimentally, so experimentalists have modified

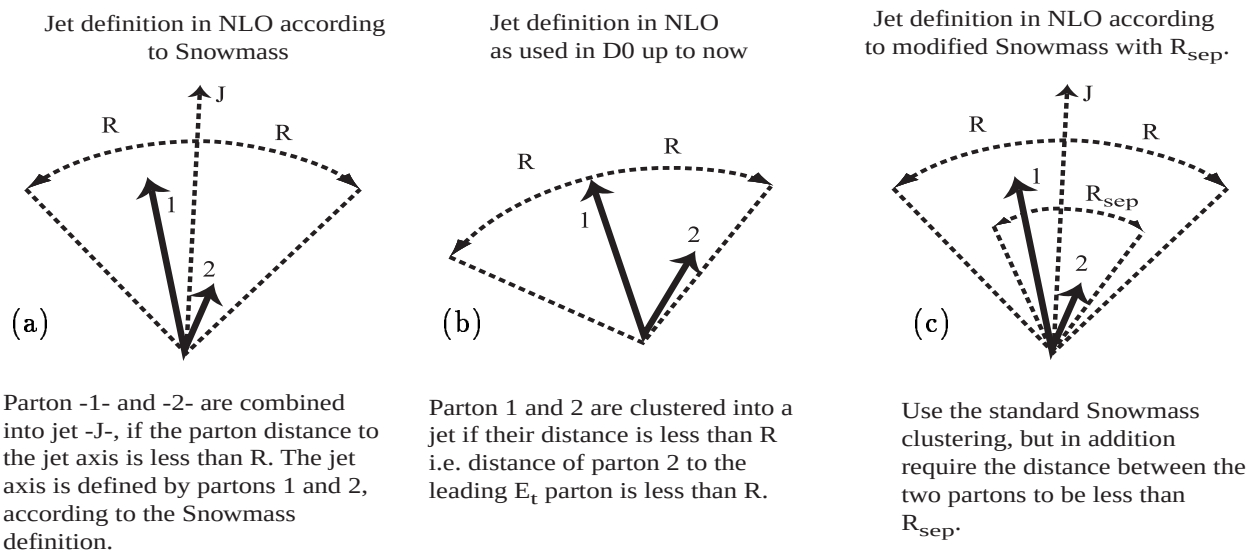

Figure 1: Illustration and description of the jet definitions at NLO parton level as used by the DØ experiment

the parton level algorithm for application in actual events. The Snowmass definition for jet direction (η, ϕ) and transverse energy (E_T) are specified as follows:

$$\eta_{jet} = \frac{\sum_i E_T^i \eta^i}{\sum_i E_T^i} \;\; ; \;\; \phi_{jet} = \frac{\sum_i E_T^i \phi^i}{\sum_i E_T^i} \;\; ; \;\; E_T = \sum_i E_T^i = \sum_i E_i \sin(\theta_i) \tag{1}$$

Here i runs over all clusters in the jet. The clustering algorithm at the NLO parton level is illustrated in Fig. 1a. For a pair of partons, the jet direction is determined using Eq. 1. If a parton is within a distance R from the reconstructed jet axis, it belongs to the jet. Here R is the chosen jet cone size and the total width of the jet cone is $2R$. At this level, splitting and merging of overlapping jets is not an issue since there are too few partons for splitting or merging to occur.

2.2 Experimental jet definitions.

At the calorimeter level in the DØ experiment, jets are defined in two steps. In the first or clustering step, all the energy that belongs to a jet is accumulated and in the second step the η, ϕ and E_T of the jet are defined. The clustering consists of the following steps:

1) Calorimeter towers $(\Delta\eta \times \Delta\phi = 0.1 \times 0.1)$ with $E_T > 1$ GeV are enumerated. Starting with the highest E_T tower, preclusters are formed using a nearest neighbor algorithm around these seed towers. Only preclusters with $E_T > 1$ GeV are used to reduce the possible number of starting points for the jet algorithm.

2) The jet direction (η,ϕ) is calculated using Eq. 1 from the energy deposit pattern in a fixed cone of size R (here R is the size of the final cone size used) around the precluster center.

3) Accumulate the energy in a cone of size R around the jet and redetermine η, ϕ.

4) Iterate steps 2 and 3 until the jet direction is stable. This is typically achieved in two or three iterations.

5) Retain only those jets with $E_T > 8$ GeV.

The issues of merging and splitting of jets will be discussed later. Up to this point (clustering) everything is identical to the Snowmass accord. All energy within a distance R from the jet axis has been collected. For DØ analyses published before 1996, the final η and ϕ of the jet differ from the Snowmass accord. The jet direction was defined as:

$$\begin{aligned} \theta_{jet} &= \tan^{-1}\left(\frac{\sqrt{(\sum_i E_x^i)^2 + (\sum_i E_y^i)^2}}{\sum_i E_z^i}\right) \\ \phi_{jet} &= \tan^{-1}\left(\frac{\sum_i E_y^i}{\sum_i E_x^i}\right) \\ \eta_{jet} &= -\ln(\tan(\theta_{jet}/2)) \end{aligned} \tag{2}$$

where

$$E_x = E_i \sin(\theta_i)\cos(\phi_i) \;\; ; \;\; E_y = E_i \sin(\theta_i)\sin(\phi_i) \;\; ; \;\; E_z = E_i \cos(\theta_i)$$

The sum over i is over all towers that are within the jet radius R.

This definition differs from the Snowmass convention in the variables ϕ_{jet} and η_{jet} as a result of early DØ Monte Carlo [3] studies. Using jets defined at the parton shower, particle and calorimeter tower level, Eq. 2 was found to give slightly better agreement between the three levels, especially in the forward rapidity regions. The definition of the transverse energy is identical to the Snowmass accord.

After publication of the measured transverse energy profiles [4] in jets, the DØ jet direction definitions were shown to cause problems at the NLO parton level, especially in the forward region. The problems at NLO arose due to an inconsistency between the definition of E_T shown in Equation 1 and the definition of η shown in Equation 2. The comparisons at the NLO parton level were done [5] by determining the jet direction with three different methods:

- Addition of the partons as four vectors
- Snowmass, Eq. 1
- DØ definitions, Eq. 2.

If four-vector addition of the partons is used as the jet finding procedure, it was shown that the Snowmass reconstruction is less biased than the DØ direction definitions. Based on the difficulty at NLO [5], DØ has adopted the standard Snowmass definitions. Studies have shown this change has little effect at the experimental level [4, 6]:

If experimental jets are reconstructed with either definition (Eq. 1 or Eq. 2), no significant systematic shift between the resulting directions is observed. The largest difference seen is a shift of ≈ 0.05 in η at high η. The same holds for jets reconstructed from HERWIG

[7] parton showers or reconstructed from the HERWIG particle level. A difference in the direction only occurs at the NLO parton level.

It should be noted that after the jet has been clustered the variables E_x, E_y and E_z measured from the jet energy depositions are available for analysis. However, if E_x, E_y, and E_z are now recalculated from η, ϕ and E_T determined from Snowmass they will *not* agree with the measured E_x, E_y, and E_z. A comparison of the "old" and "new" jet directions is given in Appendix A.

2.3 DØ Theoretical Jet Definition

For theoretical predictions, in the past DØ had used an algorithm which requires the two partons forming a jet to be within a distance R of each other. This was done because the seed tower required in the DØ experimental jet algorithm was thought of as a seed parton at the parton level. In this case the other parton has to be within R of the seed parton. This is illustrated in Fig. 1b. However we believe that this picture is incorrect. The seed tower used in the DØ experimental algorithm is simply a convenient and fast way to start the algorithm. The seed tower should not be thought of as the seed parton. We conclude that these theory predictions should not be used further. Only a modified Snowmass algorithm, which accounts for parton proximity, should be used for theory comparisons. As will be shown, this new algorithm attempts to deal with merging/splitting of jets at the parton level.

2.4 The modified Snowmass jet definition with R_{sep}

In the Snowmass algorithm as described above and in Fig. 1, the partons contributing to a jet can have a maximum separation of $2R$. Consider a two parton final state, with the partons separated by $2R$. The experimentally observed energy pattern will be determined by these two partons generating a parton shower, followed by a hadronization process and subsequent shower widening in the calorimeter. After applying the experimental jet algorithm to this object it is not clear how this state will be described with a fixed cone algorithm with cone R. Depending on the splitting and merging criteria used, such a parton configuration can be classified as one or two jets in the experiment.

This example illustrates the different treatment of jets at the parton and calorimeter level. Experimentally one makes a decision whether two jets are combined into one jet or kept as two different jets based on different criteria than at the parton level. Again, the Snowmass accord gives a prescription for this procedure, but it is not unique and is not always followed. To accommodate the differences between the jet definition at the parton and calorimeter level, an additional, purely phenomenological, parameter has been suggested by S. Ellis [1]. The variable is called R_{sep} and is the maximum allowed distance (ΔR) between two partons in a parton jet, divided by the cone size used: $R_{sep} = \Delta R/R$. This is illustrated in Fig. 1c and this algorithm will be referred to as the modified Snowmass algorithm.

The value of R_{sep} depends on details of the jet algorithm used in each experiment. Although the variable can depend on many subtle details, we expect that its value is mostly determined by the exact splitting and merging criteria used. In DØ we use the following splitting and merging algorithm: *Two jets are merged into one jet if more than 50% of the*

E_T of the jet with the smaller E_T is contained in the overlap region. The direction of the new jet is defined from the two original jets using Eq.2. If less than 50% of the E_T is contained in the overlap region, the jets are split into two distinct jets and the energy of each calorimeter cell in the overlap region is assigned to the nearest jet and the jet directions are recalculated.

At the parton level R_{sep} is the distance between two partons where we switch from a one jet to a two jet final state, even though both partons are contained within the jet defining cone. So for distances less than R_{sep} the two partons correspond to one jet and for distances larger than R_{sep} we have two jets. The value of R_{sep} is not known a priori, but it can be used to transfer the experimental splitting/merging scheme to the parton level.

The determination of R_{sep} would ideally be as follows: generate the two parton final state, apply the full showering (parton + hadronization), simulate the calorimeter response, and finally apply the experimental jet algorithm. As R_{sep} is increased at the parton level, we will observe a transition from one jet to two jet events in the simulation. The point at which this transition occurs is the value of R_{sep}. Although this method is possible, using NLO "partons" as input to shower generators is not totally without conceptual problems. Rather, we take experimentally measured jets from different events at different locations in the calorimeter and overlap them for different distances ΔR between the jet axes. Consequently the energy depositions of the two events are added together and the jet algorithm is run on the new artificial event. The value of ΔR where the event configuration switches from two jets to one jet allows a measurement of R_{sep}. This procedure has been performed with experimentally measured jets and in a more analytical way by using the jetshapes measured by DØ [4].

3 Determination of R_{sep} in DØ

3.1 R_{sep} from data

Two partons are merged into a single jet if they are within $R_{sep}\times$ (jet radius) of each other. If we assume that the jet location and energy describe those of its parent parton, we can replace the partons with jets. In this analysis a single jet from an event was overlapped onto another independent event. The single jet chosen to be placed into a different event was the first jet reconstructed with E_T greater than 20 GeV and which passed all of the standard jet quality cuts [8]. Jets which had undergone splitting or merging were not included in the sample to assure the parton-jet equivalence. The next event was chosen as the event in which the single jet would be placed. All jets in this event were required to have $E_T \geq 20$ GeV to keep the reconstruction efficiency high. The number of jets was also required to be greater than 1 and less than 6. All of the cells within the input jet were placed into the modified event and the event was re-reconstructed.

R_{sep} can be measured by plotting the difference in the number of jets before and after placement of the input jet vs the distance between the input jet and the closest jet in the modified event (ΔR). The value of ΔR at which half of the events contain an additional jet ($\Delta R_{1/2}$) was chosen as the point in which to calculate R_{sep}. R_{sep}=$\Delta R_{1/2}$/(Jet Radius).

Figure 2 shows the number of jets reconstructed from the nearest jet and the input jet vs ΔR. One can see that if the input jet is very close to another jet, only one jet is

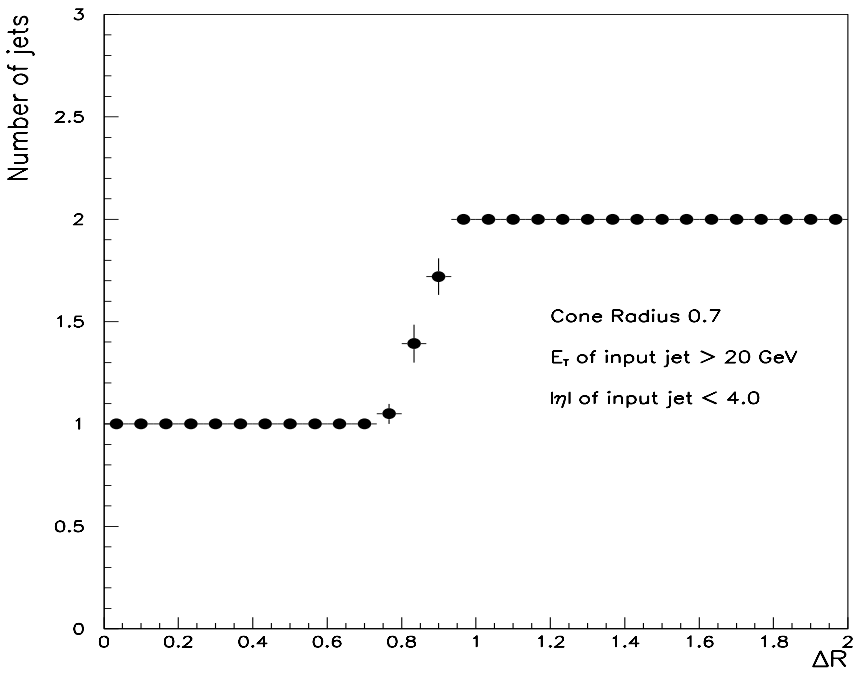

Figure 2: The number of reconstructed jets vs ΔR for a cone of radius 0.7. The input jet has $E_T \geq 20$ and $|\eta| \leq 4.0$.

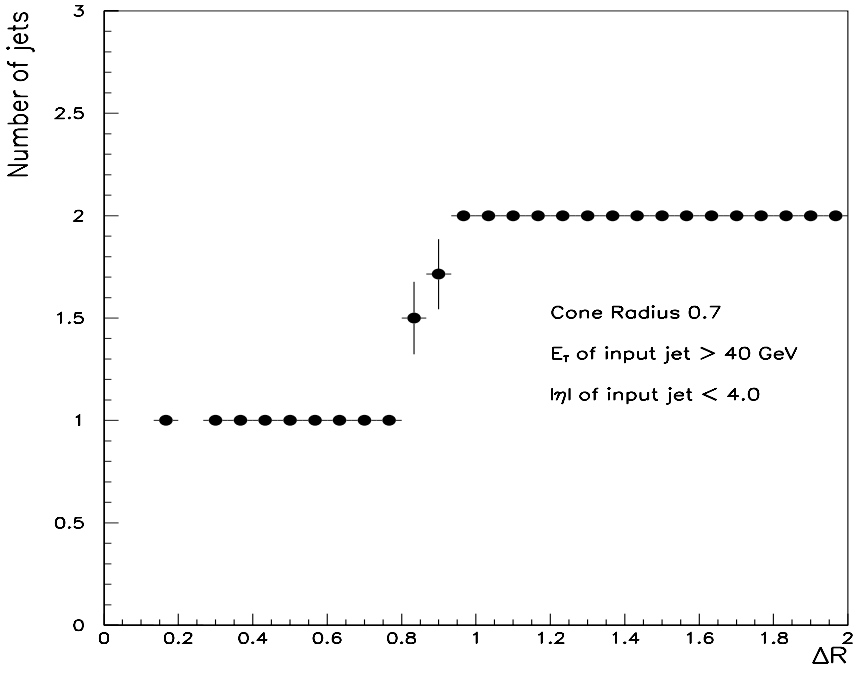

Figure 3: The number of reconstructed jets vs ΔR for a cone of radius 0.7. The input jet has $E_T \geq 40$ and $|\eta| \leq 4.0$.

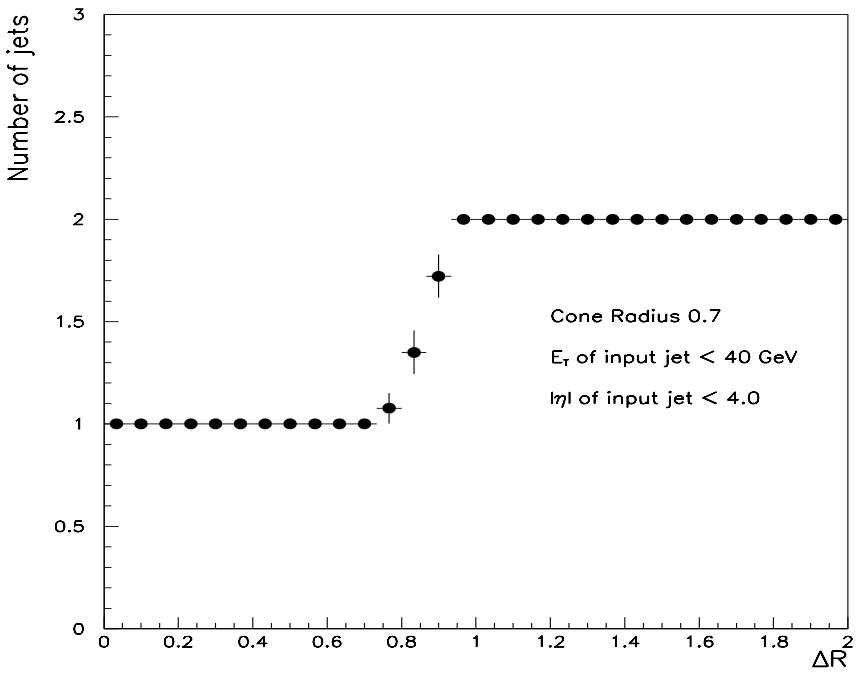

Figure 4: The number of reconstructed jets vs ΔR for a cone of radius 0.7. The input jet has $E_T \leq 40$ and $|\eta| \leq 4.0$.

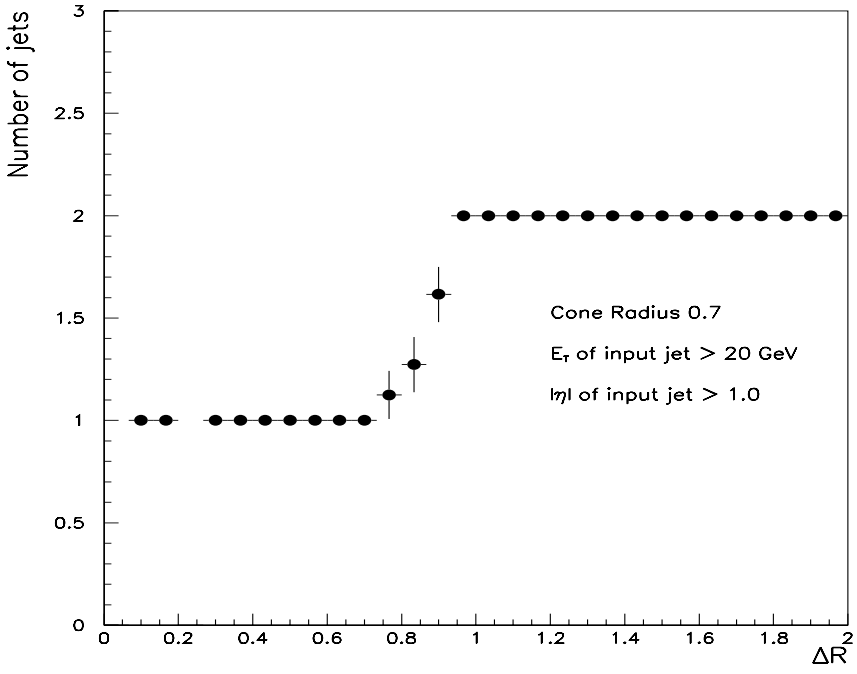

Figure 5: The number of reconstructed jets vs ΔR for a cone of radius 0.7. The input jet has $E_T \geq 20$ and $|\eta| \geq 1.0$.

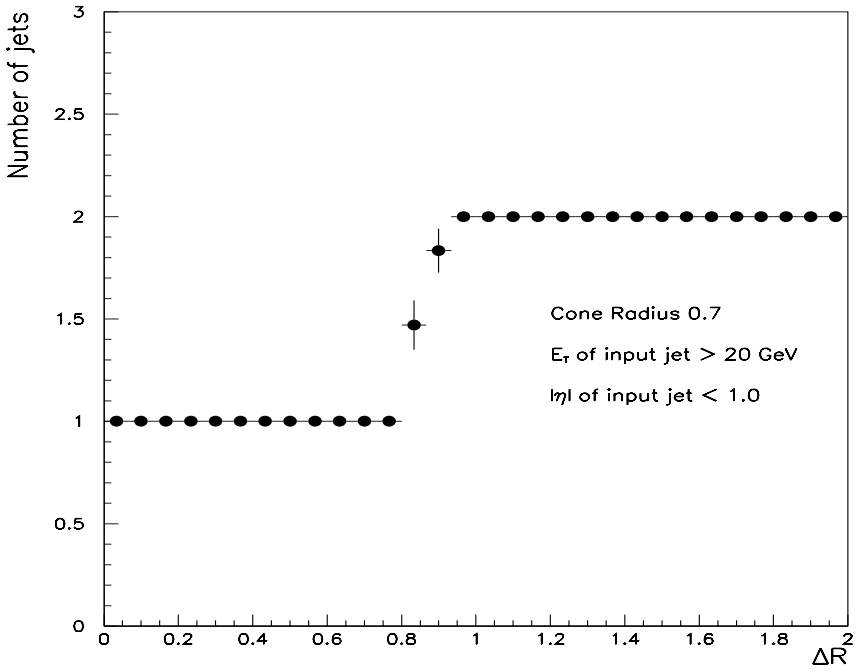

Figure 6: The number of reconstructed jets vs ΔR for a cone of radius 0.7. The input jet has $E_T \geq 20$ and $|\eta| \leq 1.0$.

reconstructed. If the input jet is far from other jets, two jets are reconstructed. In the region $0.8 \leq \Delta R \leq 1.0$, one or two jets can be reconstructed. Choosing the point at which half of the events have two reconstructed jets, yields a $\Delta R_{1/2}$ of 0.85. This value of $\Delta R_{1/2}$ gives an R_{sep} of 1.2 for a cone radius of R=0.7.

To see the effects of the input jet's E_T and η on the value of R_{sep}, four different regions were examined. Figures 3 - 6 show the transition for different input E_T and η regions. There is little dependence in R_{sep} for either E_T and η. To see the effects of a different cone size, the same procedure was performed on jets with cone size of 0.5. Figure 7 shows the effect on R_{sep} for a cone radius of 0.5. The point where half of the events contain two jets corresponds to a ΔR of 0.6, again yielding a value of $R_{sep} = 1.2$. For all of the previous plots, the event in which the input jet was placed could contain merged or split jets. To see the effects of merging and splitting on these jets, the analysis was repeated, but this time allowing no merged or split jets in the input event. After the input jet was placed in the event and re-reconstructed, merged and split jets were allowed. Figures 8 - 10 show the effects of not allowing merging and splitting on the value of R_{sep} for 3 different cone sizes. There is little effect due to merging and splitting, again all cone sizes yield values of $R_{sep} \sim 1.2$. The effects of the E_T of the input jet on R_{sep} are small. However, the effects may be diminished since the E_T of the nearest jet was not constrained. Figures 11 - 12 show the effects on R_{sep} when E_T cuts are placed on both jets. Again there is little effect on R_{sep}.

From this study of overlapping jets from different data events, we conclude that R_{sep} is nearly independent of jet conesize and not strongly dependent on the E_T of the jets. A value of R_{sep}=1.2 is the best value from this analysis.

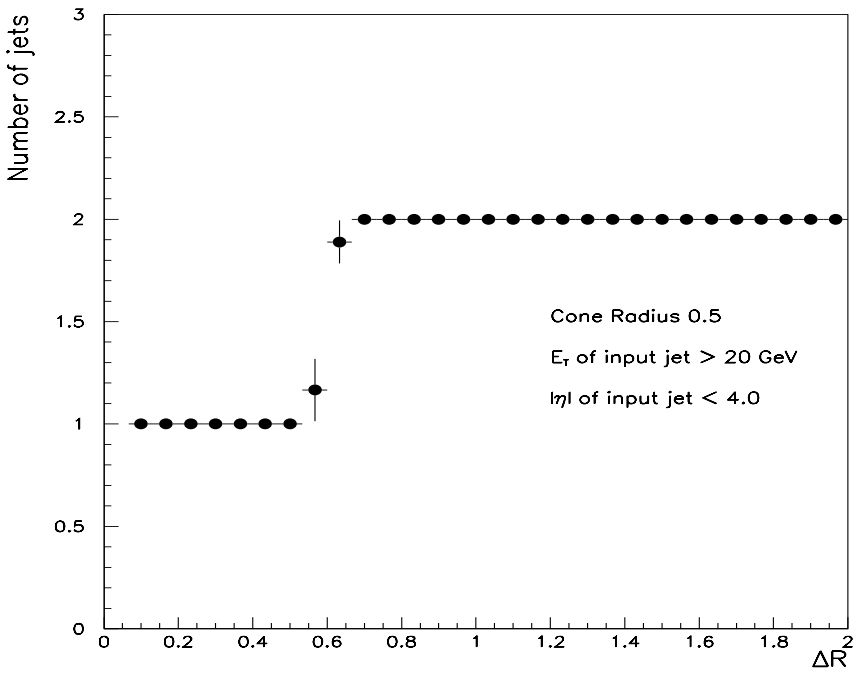

Figure 7: The number of reconstructed jets vs ΔR for a cone of radius 0.5. The input jet has $E_T \geq 20$ and $|\eta| \leq 4.0$.

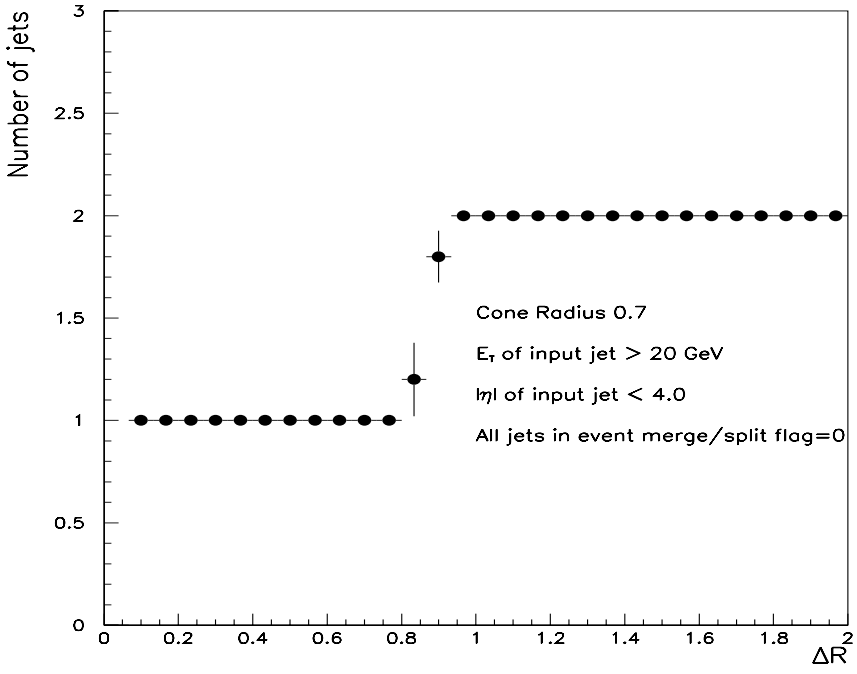

Figure 8: The number of reconstructed jets vs ΔR for a cone of radius 0.7. The input jet has $E_T \geq 20$ and $|\eta| \leq 4.0$. No merged or split jets in the input event.

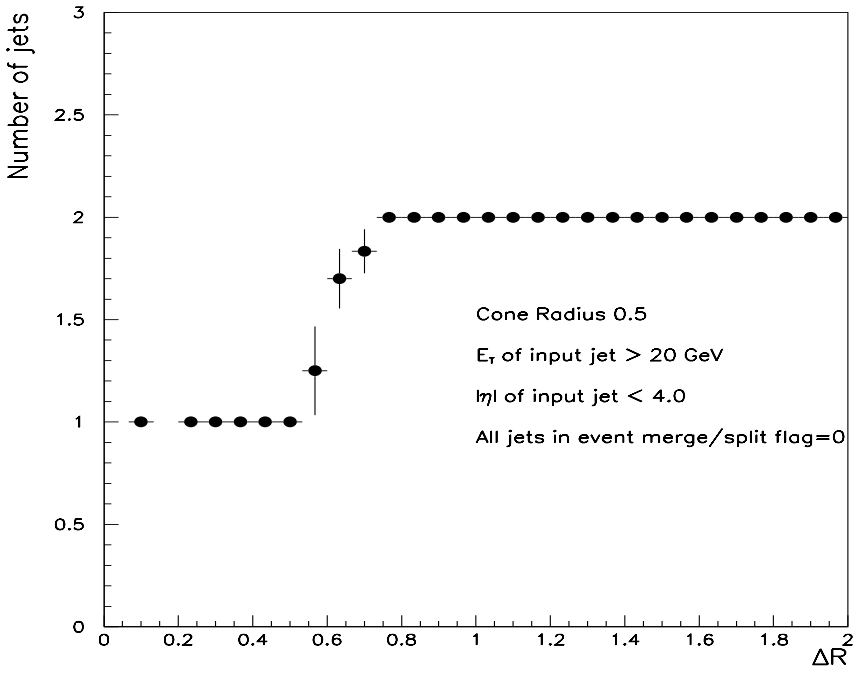

Figure 9: The number of reconstructed jets vs ΔR for a cone of radius 0.5. The input jet has $E_T \geq 20$ and $|\eta| \leq 4.0$. No merged or split jets in the input event.

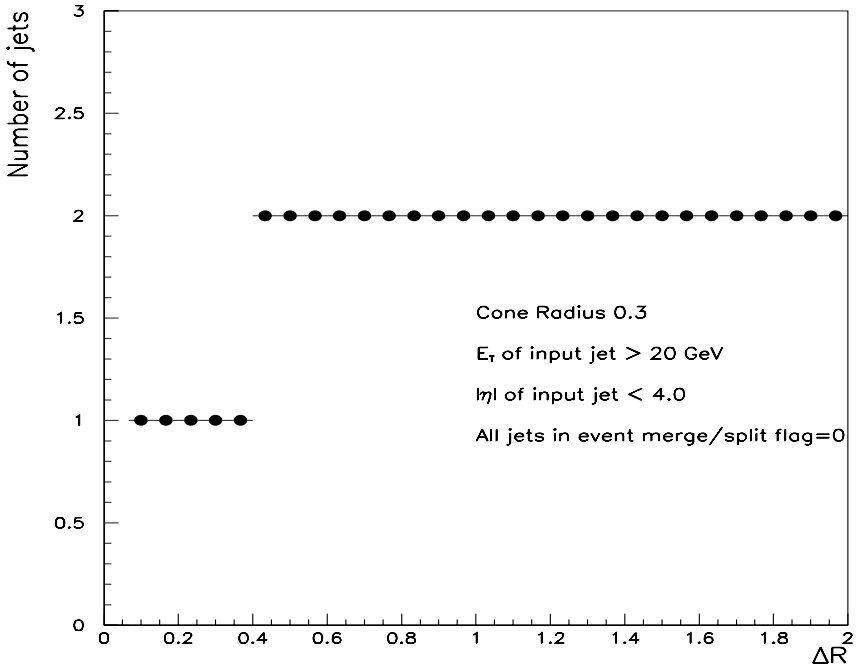

Figure 10: The number of reconstructed jets vs ΔR for a cone of radius 0.3. The input jet has $E_T \geq 20$ and $|\eta| \leq 4.0$. No merged or split jets in the input event.

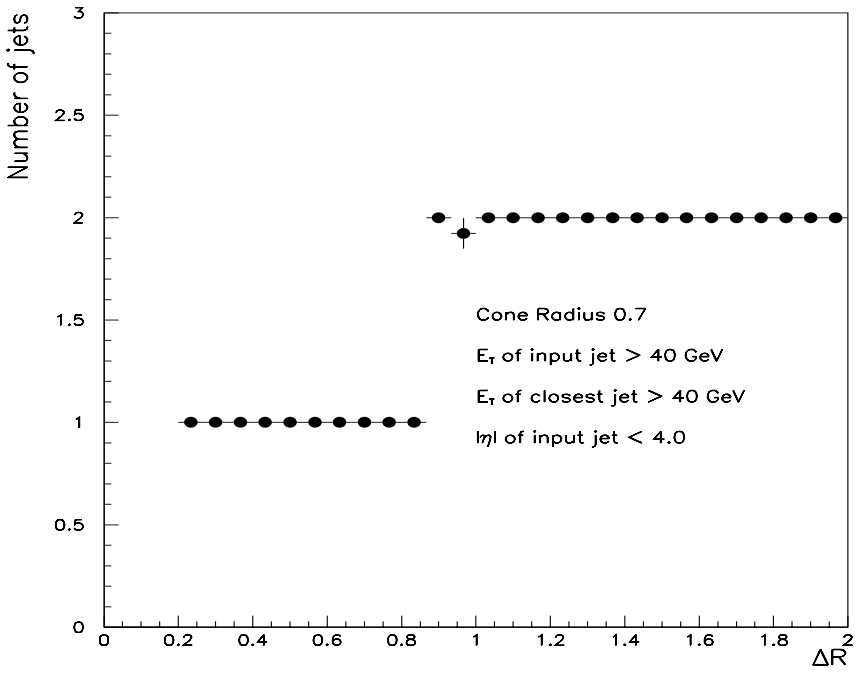

Figure 11: The number of reconstructed jets vs ΔR for a cone of radius 0.7. The input jet and the nearest jet have $E_T \geq 40$ and $|\eta| \leq 4.0$. No merged or split jets in the input event.

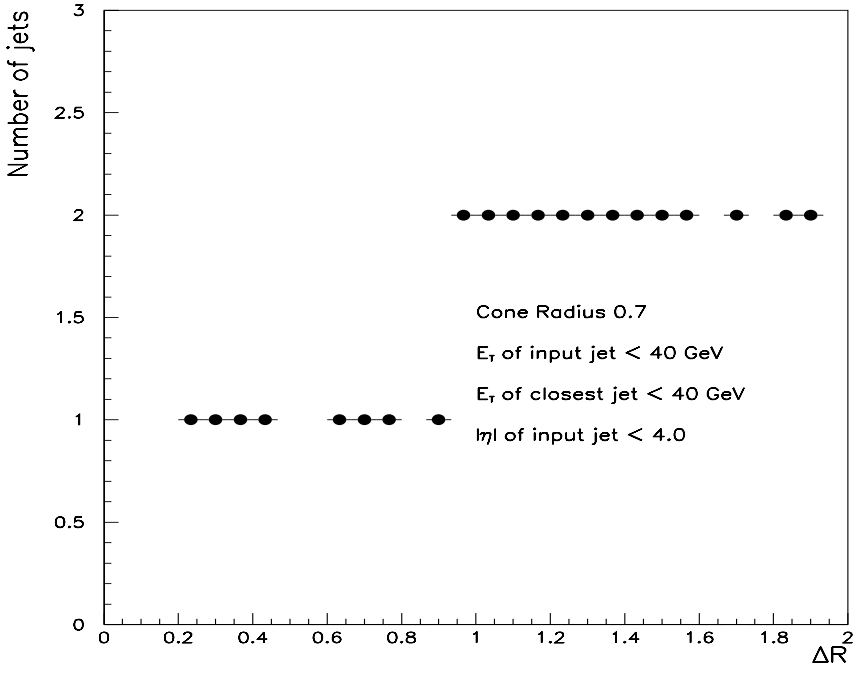

Figure 12: The number of reconstructed jets vs ΔR for a cone of radius 0.7. The input jet and the nearest jet have $E_T \leq 40$ and $|\eta| \leq 4.0$. No merged or split jets in the input event.

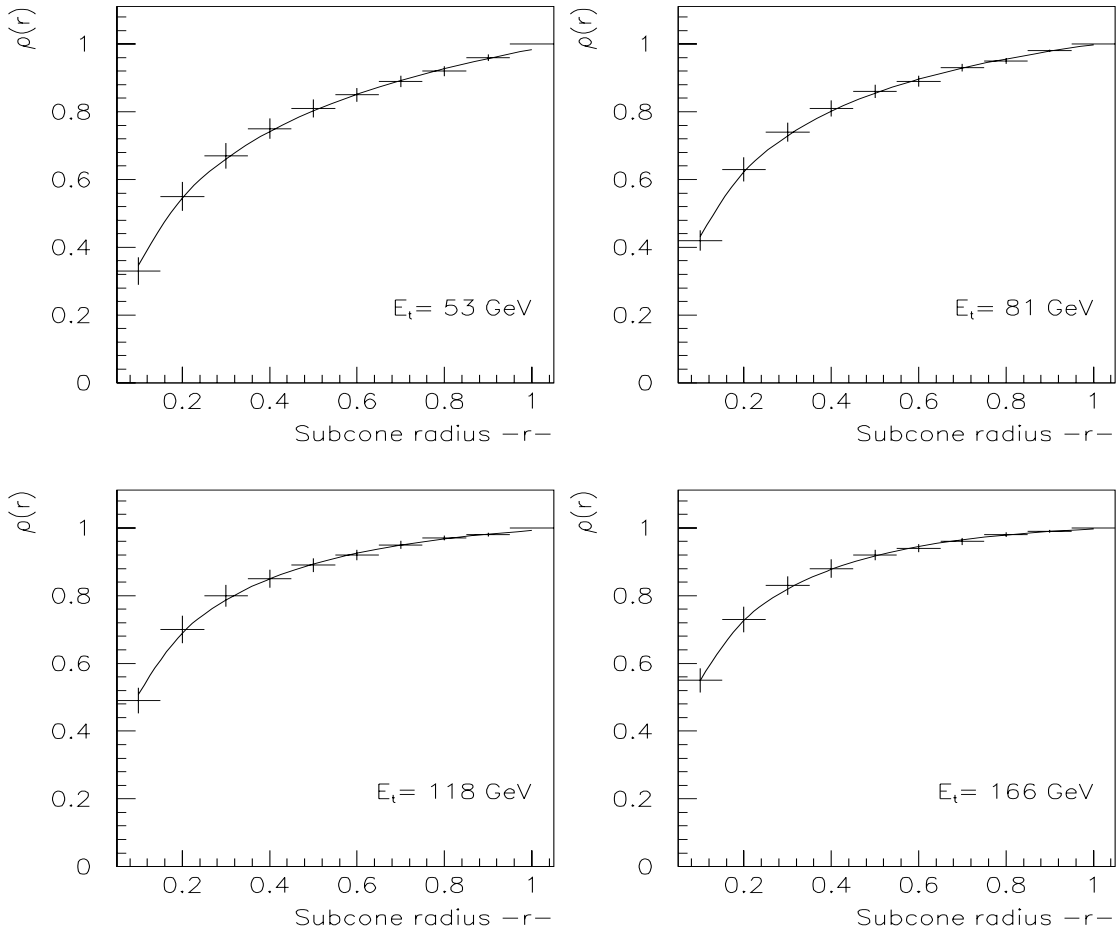

Figure 13: Fits to the DØ jet shapes as described by Equation 5 at the four E_T points.

3.2 R_{sep} from the measured jet shapes.

In a recent publication [4], DØ has published the integrated transverse energy profile of jets for several E_T's and pseudorapidities. Assuming that R_{sep} is mostly determined by the splitting and merging criteria, it should be possible to determine R_{sep} from the parameterized jet shapes as two jets approach each other.

3.2.1 Outline of the method.

Assume two jets defined by a cone size R with transverse energies E_{T1} and E_{T2} are a distance ΔR apart, where ΔR is the distance between jet axes. For $\Delta R \geq 2R$ there is no overlap between the jets. As ΔR decreases and becomes $< 2R$, the jets start overlapping. Using the convention that $E_{T2} \leq E_{T1}$, in DØ the two jets will be merged if the transverse energy in the overlap region of the two jets is $\geq 0.5 \times E_{T2}$. This will occur at a particular value of ΔR and this value is related to $R_{sep} = \Delta R/R$. So at this point the two jets will be treated as one jet (as ΔR decreases). The value of R_{sep} obviously can depend on several quantities:

- The values of E_{T1} and E_{T2}

- The jetshape or transverse energy profile of the jets
- The cone size.

To study these possible dependencies it is necessary to parameterize the transverse energy profiles of jets as a function of the distance r from the jet axis and the E_T of the jet. Given this, we can then determine R_{sep} for all possible E_{T1}, E_{T2} combinations and cone sizes.

3.2.2 Parameterization of the DØ jetshapes.

The normalized integral jetshapes as published in [4] were fitted in the central pseudorapidity region only. The jet shape, $\rho(r)$, is defined as the average fraction of calorimeter cell E_T in a subcone of radius r:

$$\rho(r) = \frac{1}{N_{jets}} \sum_{jets} \frac{E_T(r)}{E_T(r=1)}, \tag{3}$$

where N_{jets} is the number of jets in the sample. A calorimeter cell was considered to be within a subcone if the center of the cell was located within the subcone boundary. The jet shapes measure the integrated transverse energy in subcones extending from 0 to r. Given the transverse energy density in the cone as $\xi(r)$, then:

$$\rho(r) = \frac{\int_0^r \xi(r')dr'}{\int_0^1 \xi(r')dr'} \tag{4}$$

By definition, $\rho(1) = 1$. We have fitted the measured data to the following expression:

$$\rho(r) = Ar^{0.1} + Br^{0.3} + Cr^{0.5} + Dr^{0.7} + Er^{0.9} \tag{5}$$

with

$$\begin{aligned} A(E_T) &= -3.47 + 0.85 \times 10^{-2} E_T - 0.25 \times 10^{-4} E_T^2 \\ D(E_T) &= 3.30 - 0.77 \times 10^{-2} E_T + 0.22 \times 10^{-4} E_T^2 \\ B = 9.75 \;\; &; \;\; C = -8.32 \;\; ; \;\; E = -0.30 \end{aligned} \tag{6}$$

The E_T dependence of the jetshape is completely described by the energy dependence of the parameters A and D. The data used for fitting the above parameters are shown in Fig. 13. The jet shapes were measured at average transverse energies 53 (45-70), 81 (70-105), 118 (105-140), 166 (>140) GeV, where the numbers in parentheses indicate the E_T range used. Overlaid on the figure is the parameterization given by Eq. 5 and 6. The parameterization describes the experimental data very well (no surprise given 5 parameters and 10 data points at each energy point). The E_T dependence of the parameters A and D was obtained from the fits to the jet shapes at the different E_T points and is displayed in Fig. 14. These points were then fit to get the functional form of the E_T dependence as given in Eq.6. It should be noted that this form is used to obtain the jet shapes at transverse energies where it has not been measured yet (i.e. below 50 GeV and above 170 GeV). The extrapolation to lower transverse energies seems fine, but at large transverse energies it fails. The jetshape for $E_T >$ 170 GeV remains the same as at 170 GeV.

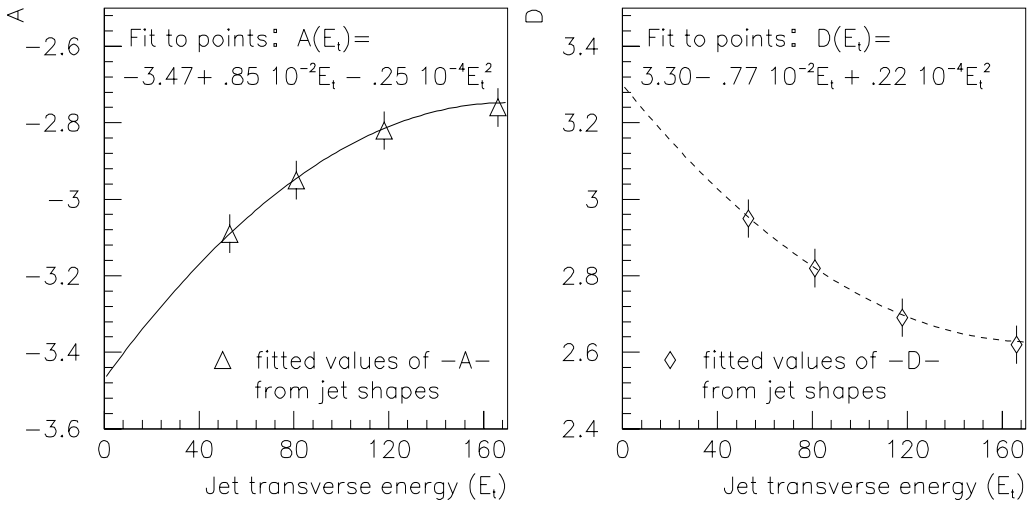

Figure 14: Fits to the E_T dependence of the parameters A and D as given by Equation 6.

3.2.3 Results on R_{sep} from jet shapes

Given these parameterizations of the jet shapes (for a jet defined using a cone size=1.0), we can parameterize the energy in the overlap region of two jets as a function of their distance ΔR. This can be done for different combinations of E_{T1} and E_{T2}, as well as for different choices of cone sizes. In addition to this, we can fix the jet shape at a particular E_T, but give the jet a different transverse energy (i.e. an $E_T = 20$ GeV jet can have the jetshape of a 50 GeV jet). The following nomenclature has been used for the R_{sep} variable:

- R_{sep}^{uni} is R_{sep} determined assuming that the transverse energy per unit area is independent of the distance from the jet axis i.e. it is uniform within the cone.
- R_{sep}^{fix} is R_{sep} determined assuming that the jetshape of all jets at all transverse energies are the same as the jetshape of a jet of $E_T = 50$ GeV.
- R_{sep}^{shape} is R_{sep} determined using the parameterized jetshape as given by Eqs. 5 and 6 at each E_T. This is the most interesting quantity.

Table 1 displays the values of R_{sep} for $30 < E_{T1} < 200$ GeV, for a variety of E_{T2} values. The range of E_{T1} was chosen such that the jet shapes are reliable and we do not extrapolate too far into unmeasured regions. The resulting values for R_{sep} are remarkably insensitive to most changes. They do not depend very much on the cone size or the jet shape. The variables $R_{sep}^{uni}, R_{sep}^{fix}$ and R_{sep}^{shape} only differ when E_{T2}/E_{T1} is very small. Comparing R_{sep}^{uni}, R_{sep}^{fix} and R_{sep}^{shape}, we observe that using the correct transverse energy dependence of the jet shapes only makes a difference at small values of E_{T2}/E_{T1}.

The only variation that is observed is the decreasing of R_{sep} with increasing E_{T2}/E_{T1}. This seems to make it impossible to use a single value for R_{sep} for all combinations. Figure 15 displays this graphically for a cone size of 0.7. Especially at low E_{T2}/E_{T1} the value increases

Table 1: The values of R_{sep} obtained from applying the DØ merging/splitting algorithm to parameterized jetshapes, for different cone sizes and parton energies.

E_{T1}	E_{T2}	R	R_{sep}^{uni}	R_{sep}^{fix}	R_{sep}^{shape}	R	R_{sep}^{uni}	R_{sep}^{fix}	R_{sep}^{shape}	R	R_{sep}^{uni}	R_{sep}^{fix}	R_{sep}^{shape}
30.	10.	0.7	1.55	1.37	1.43	0.5	1.55	1.39	1.45	0.3	1.55	1.43	1.49
30.	15.	0.7	1.45	1.30	1.35	0.5	1.45	1.32	1.38	0.3	1.45	1.36	1.42
30.	20.	0.7	1.37	1.26	1.30	0.5	1.37	1.28	1.33	0.3	1.37	1.32	1.37
30.	25.	0.7	1.32	1.23	1.27	0.5	1.32	1.25	1.29	0.3	1.32	1.29	1.33
30.	30.	0.7	1.27	1.21	1.24	0.5	1.27	1.23	1.26	0.3	1.27	1.26	1.30
40.	10.	0.7	1.61	1.42	1.46	0.5	1.61	1.45	1.48	0.3	1.61	1.49	1.52
40.	20.	0.7	1.45	1.30	1.34	0.5	1.45	1.32	1.36	0.3	1.45	1.36	1.40
40.	30.	0.7	1.34	1.24	1.27	0.5	1.34	1.26	1.29	0.3	1.34	1.30	1.33
40.	40.	0.7	1.27	1.21	1.22	0.5	1.27	1.23	1.25	0.3	1.27	1.26	1.28
50.	10.	0.7	1.66	1.47	1.48	0.5	1.66	1.49	1.51	0.3	1.66	1.53	1.54
50.	20.	0.7	1.50	1.34	1.36	0.5	1.50	1.36	1.38	0.3	1.50	1.40	1.42
50.	30.	0.7	1.40	1.27	1.29	0.5	1.40	1.30	1.31	0.3	1.40	1.33	1.35
50.	40.	0.7	1.33	1.23	1.24	0.5	1.33	1.26	1.26	0.3	1.33	1.29	1.30
50.	50.	0.7	1.27	1.21	1.21	0.5	1.27	1.23	1.23	0.3	1.27	1.26	1.26
80.	10.	0.7	1.74	1.56	1.53	0.5	1.74	1.58	1.55	0.3	1.74	1.61	1.59
80.	20.	0.7	1.61	1.42	1.40	0.5	1.61	1.45	1.43	0.3	1.61	1.49	1.47
80.	30.	0.7	1.52	1.35	1.33	0.5	1.52	1.37	1.35	0.3	1.52	1.41	1.39
80.	40.	0.7	1.45	1.30	1.28	0.5	1.45	1.32	1.30	0.3	1.45	1.36	1.34
80.	50.	0.7	1.39	1.27	1.24	0.5	1.39	1.29	1.27	0.3	1.39	1.33	1.30
80.	60.	0.7	1.34	1.24	1.22	0.5	1.34	1.26	1.24	0.3	1.34	1.30	1.27
80.	70.	0.7	1.30	1.22	1.19	0.5	1.30	1.24	1.21	0.3	1.30	1.28	1.25
80.	80.	0.7	1.27	1.21	1.17	0.5	1.27	1.23	1.20	0.3	1.27	1.26	1.23
100.	10.	0.7	1.77	1.60	1.54	0.5	1.77	1.62	1.57	0.3	1.77	1.65	1.62
100.	30.	0.7	1.57	1.39	1.34	0.5	1.57	1.41	1.37	0.3	1.57	1.45	1.42
100.	50.	0.7	1.45	1.30	1.26	0.5	1.45	1.32	1.29	0.3	1.45	1.36	1.33
100.	70.	0.7	1.36	1.25	1.21	0.5	1.36	1.27	1.23	0.3	1.36	1.31	1.27
100.	90.	0.7	1.30	1.22	1.17	0.5	1.30	1.24	1.19	0.3	1.30	1.28	1.23
150.	10.	0.7	1.82	1.67	1.57	0.5	1.82	1.69	1.62	0.3	1.82	1.72	1.67
150.	40.	0.7	1.60	1.41	1.32	0.5	1.60	1.43	1.37	0.3	1.60	1.47	1.42
150.	70.	0.7	1.47	1.31	1.24	0.5	1.47	1.34	1.27	0.3	1.47	1.37	1.32
150.	100.	0.7	1.37	1.26	1.18	0.5	1.37	1.28	1.21	0.3	1.37	1.32	1.26
150.	130.	0.7	1.31	1.22	1.15	0.5	1.31	1.25	1.18	0.3	1.31	1.28	1.22
200.	20.	0.7	1.77	1.60	1.49	0.5	1.77	1.62	1.54	0.3	1.77	1.65	1.60
200.	60.	0.7	1.57	1.39	1.30	0.5	1.57	1.41	1.34	0.3	1.57	1.45	1.39
200.	100.	0.7	1.45	1.30	1.22	0.5	1.45	1.32	1.25	0.3	1.45	1.36	1.30
200.	140.	0.7	1.36	1.25	1.17	0.5	1.36	1.27	1.20	0.3	1.36	1.31	1.25
200.	180.	0.7	1.30	1.22	1.14	0.5	1.30	1.24	1.17	0.3	1.30	1.28	1.22

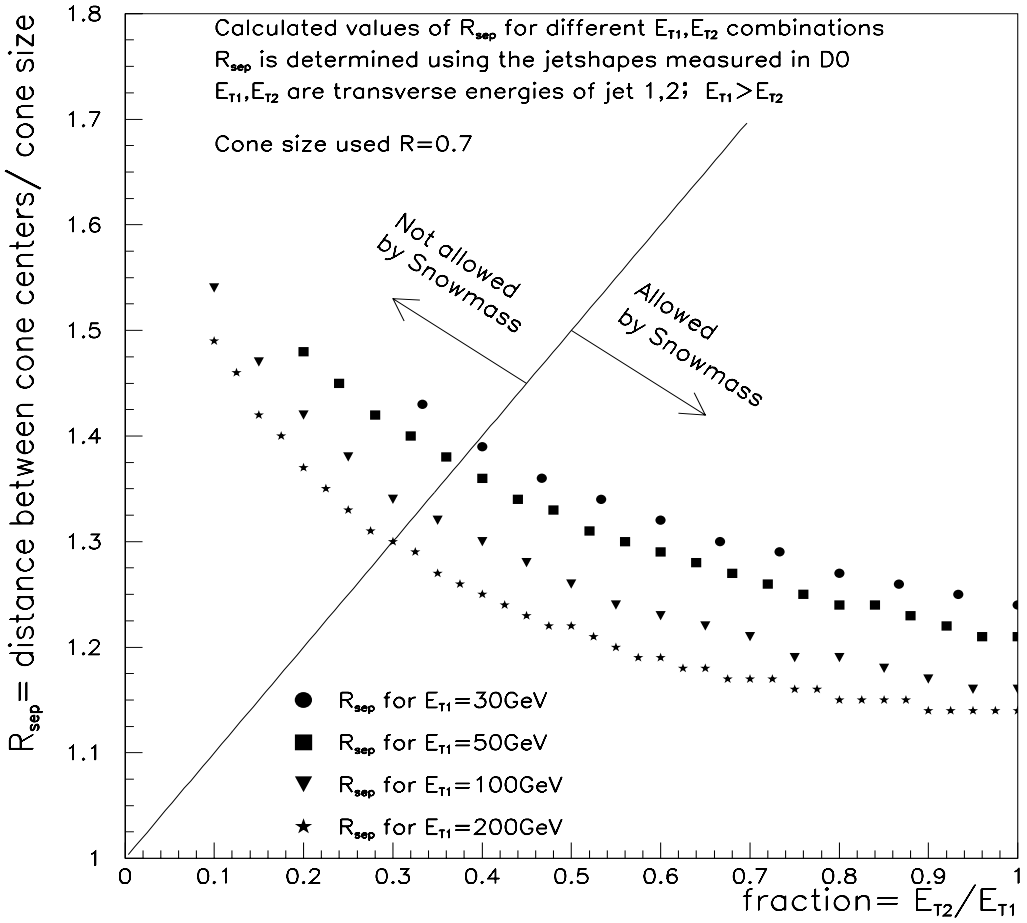

Figure 15: The value of R_{sep} as a function of the parton transverse energies E_{T1}, E_{T2}. Shown are the maximum values allowed by the Snowmass algorithm (solid line) and the experimental splitting and merging algorithm(symbols). The results shown are for R=0.7.

rapidly. However, such large values of R_{sep} are not allowed by the Snowmass algorithm itself. This is discussed in the next section.

3.3 Limits on values of R_{sep} from the algorithm.

R_{sep} has been introduced as a phenomenological parameter at the parton level that can be adjusted to accommodate different merging and splitting algorithms. However the distance between two partons that are combined into a jet using the Snowmass definitions is limited and can not always be $2R$. Depending on the transverse energies of the partons involved the distance is much smaller than $2R$. So some of the E_{T1} and E_{T2} combinations in Table 1 are unphysical and not allowed. To determine the maximum distance allowed between two partons in the Snowmass algorithm, consider two partons with: $E_{T1}, E_{T2}, \eta_1, \eta_2$ and $\phi_1 = \phi_2 = 0$. If we introduce $f = E_{T2}/E_{T1}$ the jet pseudorapidity is given by:

$$\eta_{jet} = \frac{E_{T1}\eta_1 + E_{T2}\eta_2}{E_{T1} + E_{T2}} = \frac{\eta_1 + f\eta_2}{1+f}$$
$$\eta_{jet}(1+f) = \eta_1 + f\eta_2 \tag{7}$$

We assume for simplicity that $E_{T2} < E_{T1}$ and that $\eta_1, \eta_2 > 0$ and that $\eta_2 > \eta_1$. This implies that $\eta_{jet} > 0$ and is between η_1 and η_2. It also makes it somewhat easier to calculate the maximum distance between the partons if they form a jet. The criteria for them to be combined into a jet are:

$$\eta_{jet} - \eta_1 \leq R \text{ and } \eta_2 - \eta_{jet} \leq R \tag{8}$$
$$\tag{9}$$

The distance (ΔR) between the two partons is:

$$\Delta R = \eta_2 - \eta_1 = \eta_2 - (1+f)\eta_{jet} + f\eta_2$$
$$\Delta R = (1+f)(\eta_2 - \eta_{jet}) \leq (1+f)R \tag{10}$$

The maximum distance between the two partons increases linearly with f which results in:

$$R_{sep} = \Delta R/R \leq 1 + f. \tag{11}$$

So the limits are $R_{sep} = 1$ in the case that $E_{T2} \to 0$ and $R_{sep} = 2$ in the case $E_{T2} \to E_{T1}$.

The large values obtained for R_{sep} in Table 1 at very low values of E_{T2}/E_{T1} can be ignored if they do not satisfy the condition $R_{sep} \leq 1 + f$, because the algorithm would never allow such large distances between two partons. To reflect this additional constraint on R_{sep}, Table 2 displays the smallest value of R_{sep}, resulting either from the merging and splitting algorithm or Eq. 11. To indicate where the limit comes from, the value for R_{sep} is negative if is determined by Eq. 11.

Graphically this is presented in Figure 15. The solid line in this figure shows the maximum value allowed for R_{sep} by Eq. 11 as a function of E_{T2}/E_{T1}. The symbols show the maximum value of R_{sep} as obtained by applying the DØ splitting/merging criteria to partons and given in Table 1. The plotted symbols are obtained by using the measured jetshapes for

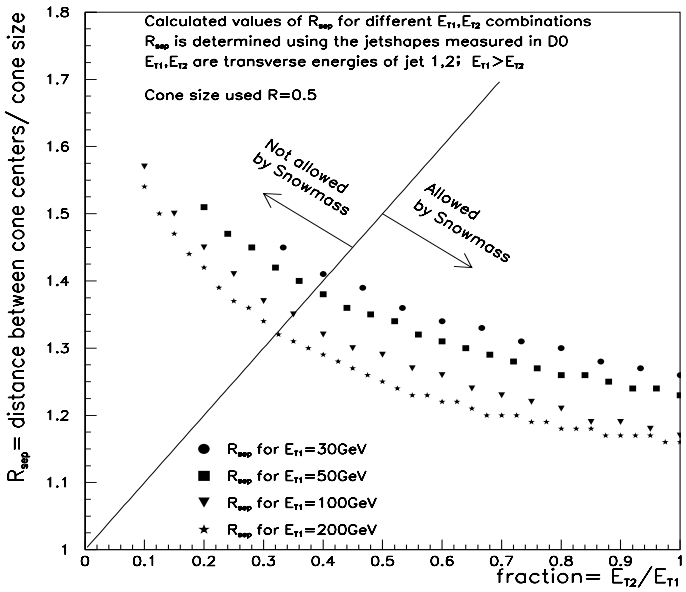

Figure 16: The value of R_{sep} as a function of the parton transverse energies E_{T1}, E_{T2}. Shown are the maximum values allowed by the Snowmass algorithm (solid line) and the experimental splitting and merging algorithm(symbols). The results shown are for R=0.5.

both partons i.e. R_{sep}^{shape} in Table 1 and a nominal cone size of R=0.7. The value obtained for R_{sep} shows a slight dependence on the E_{T1}, which is caused by the dependence of the jetshape on the jet transverse energy. All these results are for centrally produced jets. The results for the other cone sizes, 0.5 and 0.3, are shown in Figures 16 and 17

4 Theoretical predictions with different R_{sep}.

We have generated distributions of the inclusive jet cross section ($d\sigma^2/dE_T d\eta$) for different R_{sep} values using the program JETRAD [9]. The parton distributions(pdf) CTEQ2M [10] was used and $\mu = E_T$ was chosen for the renormalization/factorization scale. The distributions are plotted as a function of the E_T of the jets when such jets are in a fixed $|\eta|$ range. The range is from $|\eta| = 0.0$ to $|\eta| = 4.0$ in increments of 0.5, in other words, we have E_T distributions for $0.0 \leq |\eta| < 0.5$, $0.5 \leq |\eta| < 1.0$, $1.0 \leq |\eta| < 1.5$, $1.5 \leq |\eta| < 2.0$, $2.0 \leq |\eta| < 2.5$, $2.5 \leq |\eta| < 3.0$, $3.0 \leq |\eta| < 3.5$, and $3.5 \leq |\eta| < 4.0$. The R_{sep} values used are: 1.0, 1.1, 1.2, 1.3, 1.4, 1.5, 1.6, and 2.0. Note that R_{sep}=2.0 corresponds to the standard Snowmass case while R_{sep}=1.0 corresponds to the DØ algorithm (see section 2.3).

In order to understand the differences due to the R_{sep} value, we have taken a ratio of the E_T distributions from different R_{sep} values. Figures 18 and 19 show the ratio plots for R_{sep}=1.3 versus R_{sep}=2.0. The ratio has been fitted to a straight line and the results are shown in Table 3.

As we can see, a straight line is a good model of the ratios between the cross sections at these two R_{sep} values. In particular, for the case of $0.0 \leq |\eta| < 0.5$, the cross section with R_{sep}=1.3 is 4% lower than the cross section with R_{sep}=2.0 at $E_T = 20\ GeV$. At $E_T = 500\ GeV$, the cross section with R_{sep}=1.3 is only 1.5% lower than the cross section

Table 2: Same results as Table I, but with the with the Snowmass implicit distance constraint implied by negation.

E_{T1}	E_{T2}	R	R_{sep}^{uni}	R_{sep}^{fix}	R_{sep}^{shape}	R	R_{sep}^{uni}	R_{sep}^{fix}	R_{sep}^{shape}	R	R_{sep}^{uni}	R_{sep}^{fix}	R_{sep}^{shape}
30.	10.	0.7	-1.33	-1.33	-1.33	0.5	-1.33	-1.33	-1.33	0.3	-1.33	-1.33	-1.33
30.	15.	0.7	1.45	1.30	1.35	0.5	1.45	1.32	1.38	0.3	1.45	1.36	1.42
30.	20.	0.7	1.37	1.26	1.30	0.5	1.37	1.28	1.33	0.3	1.37	1.32	1.37
30.	25.	0.7	1.32	1.23	1.27	0.5	1.32	1.25	1.29	0.3	1.32	1.29	1.33
30.	30.	0.7	1.27	1.21	1.24	0.5	1.27	1.23	1.26	0.3	1.27	1.26	1.30
40.	10.	0.7	-1.25	-1.25	-1.25	0.5	-1.25	-1.25	-1.25	0.3	-1.25	-1.25	-1.25
40.	20.	0.7	1.45	1.30	1.34	0.5	1.45	1.32	1.36	0.3	1.45	1.36	1.40
40.	30.	0.7	1.34	1.24	1.27	0.5	1.34	1.26	1.29	0.3	1.34	1.30	1.33
40.	40.	0.7	1.27	1.21	1.22	0.5	1.27	1.23	1.25	0.3	1.27	1.26	1.28
50.	10.	0.7	-1.20	-1.20	-1.20	0.5	-1.20	-1.20	-1.20	0.3	-1.20	-1.20	-1.20
50.	20.	0.7	-1.40	1.34	1.36	0.5	-1.40	1.36	1.38	0.3	-1.40	1.40	-1.40
50.	30.	0.7	1.40	1.27	1.29	0.5	1.40	1.30	1.31	0.3	1.40	1.33	1.35
50.	40.	0.7	1.33	1.23	1.24	0.5	1.33	1.26	1.26	0.3	1.33	1.29	1.30
50.	50.	0.7	1.27	1.21	1.21	0.5	1.27	1.23	1.23	0.3	1.27	1.26	1.26
80.	10.	0.7	-1.13	-1.13	-1.13	0.5	-1.13	-1.13	-1.13	0.3	-1.13	-1.13	-1.13
80.	20.	0.7	-1.25	-1.25	-1.25	0.5	-1.25	-1.25	-1.25	0.3	-1.25	-1.25	-1.25
80.	30.	0.7	-1.38	1.35	1.33	0.5	-1.38	1.37	1.35	0.3	-1.38	-1.38	-1.38
80.	40.	0.7	1.45	1.30	1.28	0.5	1.45	1.32	1.30	0.3	1.45	1.36	1.34
80.	50.	0.7	1.39	1.27	1.24	0.5	1.39	1.29	1.27	0.3	1.39	1.33	1.30
80.	60.	0.7	1.34	1.24	1.22	0.5	1.34	1.26	1.24	0.3	1.34	1.30	1.27
80.	70.	0.7	1.30	1.22	1.19	0.5	1.30	1.24	1.21	0.3	1.30	1.28	1.25
80.	80.	0.7	1.27	1.21	1.17	0.5	1.27	1.23	1.20	0.3	1.27	1.26	1.23
100.	10.	0.7	-1.10	-1.10	-1.10	0.5	-1.10	-1.10	-1.10	0.3	-1.10	-1.10	-1.10
100.	30.	0.7	-1.30	-1.30	-1.30	0.5	-1.30	-1.30	-1.30	0.3	-1.30	-1.30	-1.30
100.	50.	0.7	1.45	1.30	1.26	0.5	1.45	1.32	1.29	0.3	1.45	1.36	1.33
100.	70.	0.7	1.36	1.25	1.21	0.5	1.36	1.27	1.23	0.3	1.36	1.31	1.27
100.	90.	0.7	1.30	1.22	1.17	0.5	1.30	1.24	1.19	0.3	1.30	1.28	1.23
150.	10.	0.7	-1.07	-1.07	-1.07	0.5	-1.07	-1.07	-1.07	0.3	-1.07	-1.07	-1.07
150.	40.	0.7	-1.27	-1.27	-1.27	0.5	-1.27	-1.27	-1.27	0.3	-1.27	-1.27	-1.27
150.	70.	0.7	1.47	1.31	1.24	0.5	1.47	1.34	1.27	0.3	1.47	1.37	1.32
150.	100.	0.7	1.37	1.26	1.18	0.5	1.37	1.28	1.21	0.3	1.37	1.32	1.26
150.	130.	0.7	1.31	1.22	1.15	0.5	1.31	1.25	1.18	0.3	1.31	1.28	1.22
200.	20.	0.7	-1.10	-1.10	-1.10	0.5	-1.10	-1.10	-1.10	0.3	-1.10	-1.10	-1.10
200.	60.	0.7	-1.30	-1.30	1.30	0.5	-1.30	-1.30	-1.30	0.3	-1.30	-1.30	-1.30
200.	100.	0.7	1.45	1.30	1.22	0.5	1.45	1.32	1.25	0.3	1.45	1.36	1.30
200.	140.	0.7	1.36	1.25	1.17	0.5	1.36	1.27	1.20	0.3	1.36	1.31	1.25
200.	180.	0.7	1.30	1.22	1.14	0.5	1.30	1.24	1.17	0.3	1.30	1.28	1.22

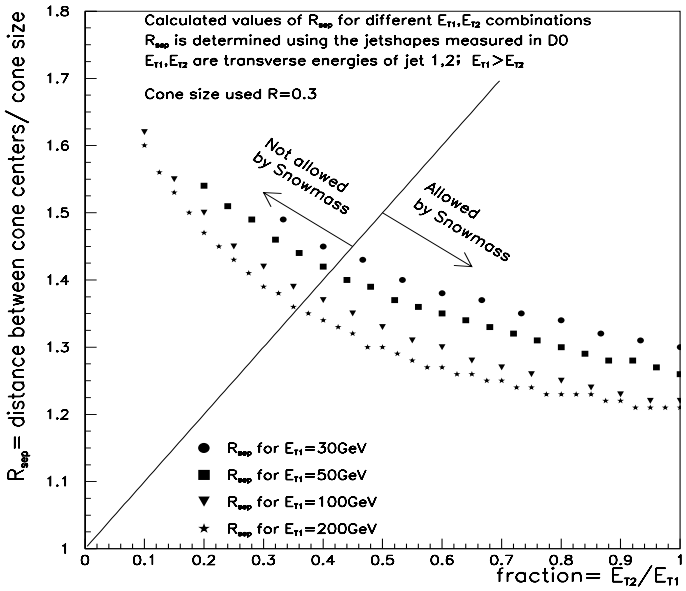

Figure 17: The value of R_{sep} as a function of the parton transverse energies E_{T1}, E_{T2}. Shown are the maximum values allowed by the Snowmass algorithm (solid line) and the experimental splitting and merging algorithm(symbols). The results shown are for R=0.3.

$\|\eta\|$ range	Intercept	Slope	χ^2/ndf
$0.0-0.5$	0.96	0.50E-4	39.9/47
$0.5-1.0$	0.96	0.54E-4	39.6/42
$1.0-1.5$	0.96	0.68E-4	26.4/32
$1.5-2.0$	0.95	0.17E-3	7.6/22
$2.0-2.5$	0.95	0.24E-3	17.5/17
$2.5-3.0$	0.94	0.30E-3	6.3/10
$3.0-3.5$	0.96	-0.32E-3	5.9/6
$3.5-4.0$	0.93	0.91E-3	1.0/2

Table 3: Outcome of fitting the R_{sep}=1.3/R_{sep}=2.0 ratio to a straight line. The first column indicates the $|\eta|$ range. The second and third column shows the intercept and slope of the fit respectively. The last column shows the goodness of the fit.

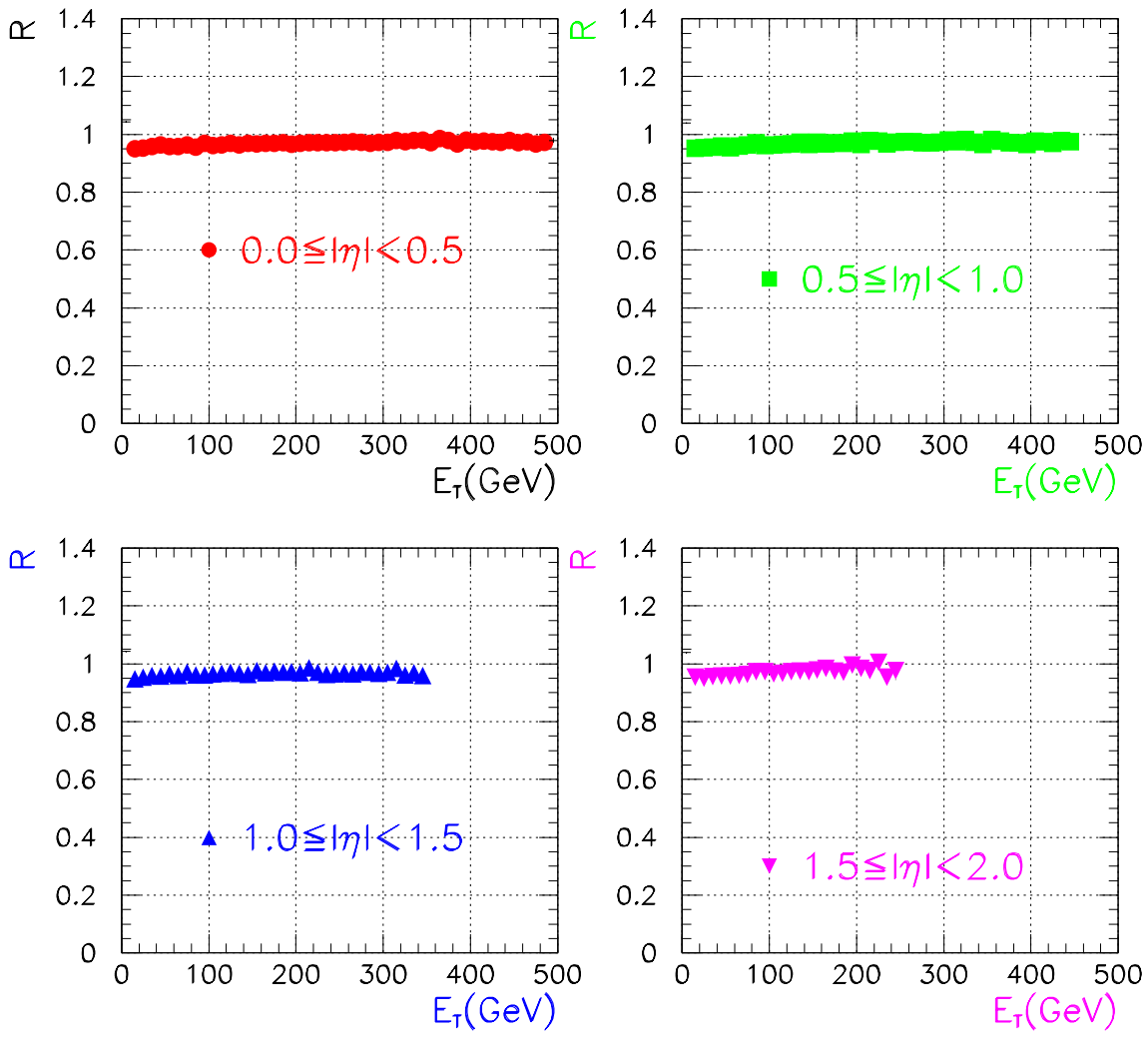

Figure 18: Ratio of R_{sep}=1.3/R_{sep}=2.0 cross sections for the four central $|\eta|$ slices.

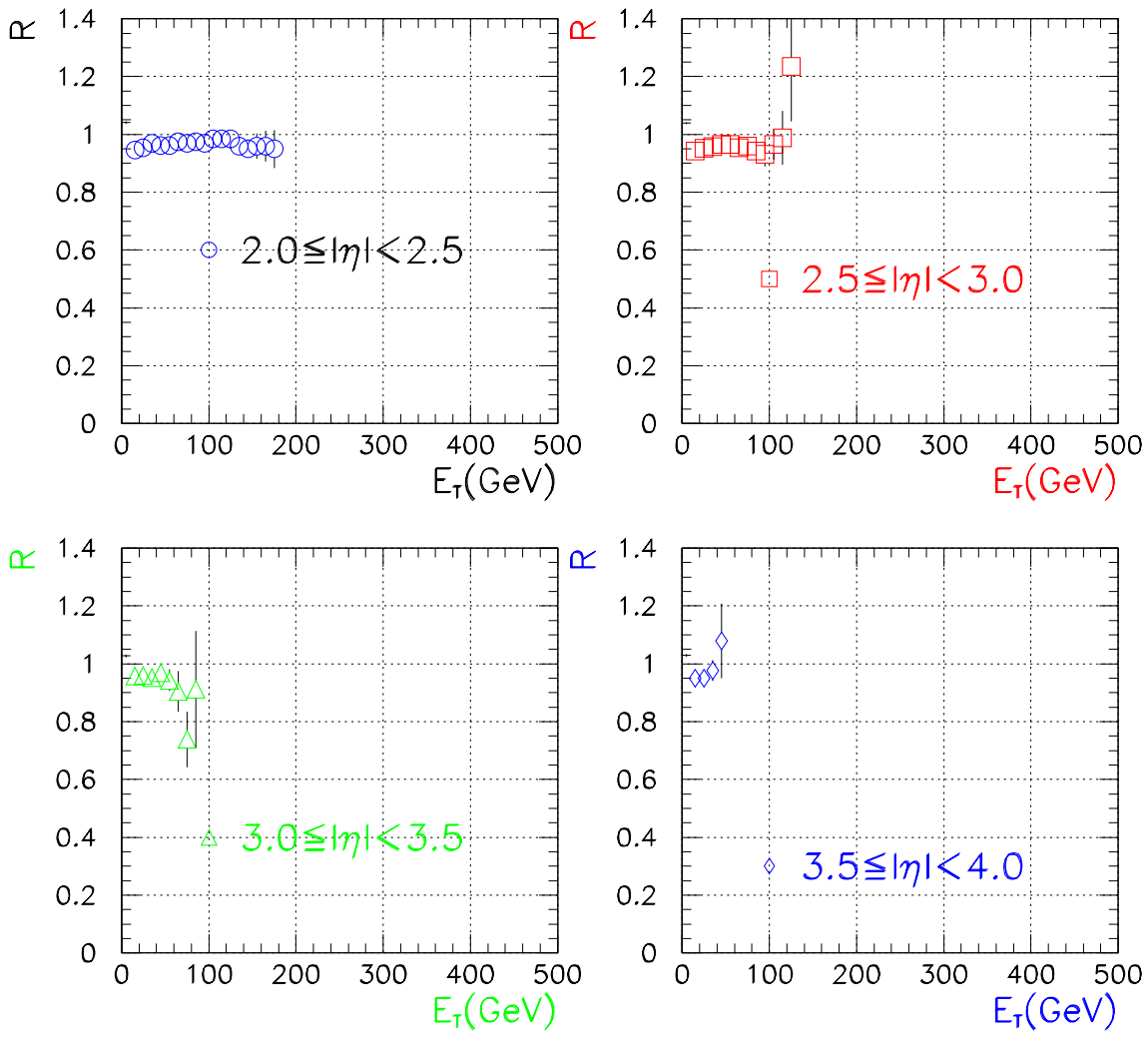

Figure 19: Ratio of R_{sep}=1.3/R_{sep}=2.0 cross sections for the four forward $|\eta|$ slices.

$\|\eta\|$ range	Intercept	χ^2/ndf
$0.0 - 0.5$	0.99	47.5/48
$0.5 - 1.0$	0.99	29.8/43
$1.0 - 1.5$	0.99	33.7/33
$1.5 - 2.0$	0.98	16.6/23
$2.0 - 2.5$	0.98	14.7/18
$2.5 - 3.0$	0.99	11.9/11
$3.0 - 3.5$	0.98	6.7/6
$3.5 - 4.0$	0.98	1.7/3

Table 4: Outcome of fitting the R_{sep}=1.2/R_{sep}=1.3 ratio to a straight horizontal line. The first column indicates the $|\eta|$ range. The second column shows the intercept of the fit and the last column shows the goodness of the fit.

with R_{sep}=2.0.

We also perform fits to the ratio of cross sections for R_{sep}=1.2 versus R_{sep}=1.3 from Figs. 20 and 21 and the results are described in Table 4. In this case, it was sufficient to fit the ratio to a straight horizontal line and it shows that there is at most a 2% difference between R_{sep}=1.2 and R_{sep}=1.3.

5 Conclusions

Values of $R_{sep} > 1.7$ in Figure 15 are rather rare because they require $E_{T2}/E_{T1} > 0.7$, which is kinematically unlikely. The more favored configuration of two partons is one with small E_{T2}/E_{T1}, which implies small values of R_{sep}. So we expect that NLO predictions are rather insensitive to choices of R_{sep} between 1.2 and 2.0 (because few combinations originate from this region), but become very dependent on it for smaller values. Considering the region allowed by the Snowmass algorithm it is obvious that the experimental merging/splitting algorithm limits R_{sep} to 1.2 to 1.4 for the jet transverse energies considered ($30 < E_{T1} < 200$ GeV). This result is to be compared with R_{sep}=1.2 which we obtained from overlaying real experimental jets (see section 3.1). The experimental overlapping of jets was done at rather low transverse energies and typically the transverse energies of the two jets were close i.e $E_{T2}/E_{T1} \approx 0.8$ to 1. In this region the results obtained from the jetshapes (section 3.2.3) also tend to be around 1.2 or lower. So we conclude that these methods agree.

Taking into account that large values of E_{T2}/E_{T1} are unlikely and that we prefer to choose one value for R_{sep} independent of jet transverse energies, we conclude that the most reasonable value is $R_{sep} = 1.3$. This value is independent of the cone size used, as shown in section 3.1. However the results derived from jetshapes and shown in Figures 16 and 17 indicate that one might use a larger value for R_{sep}.

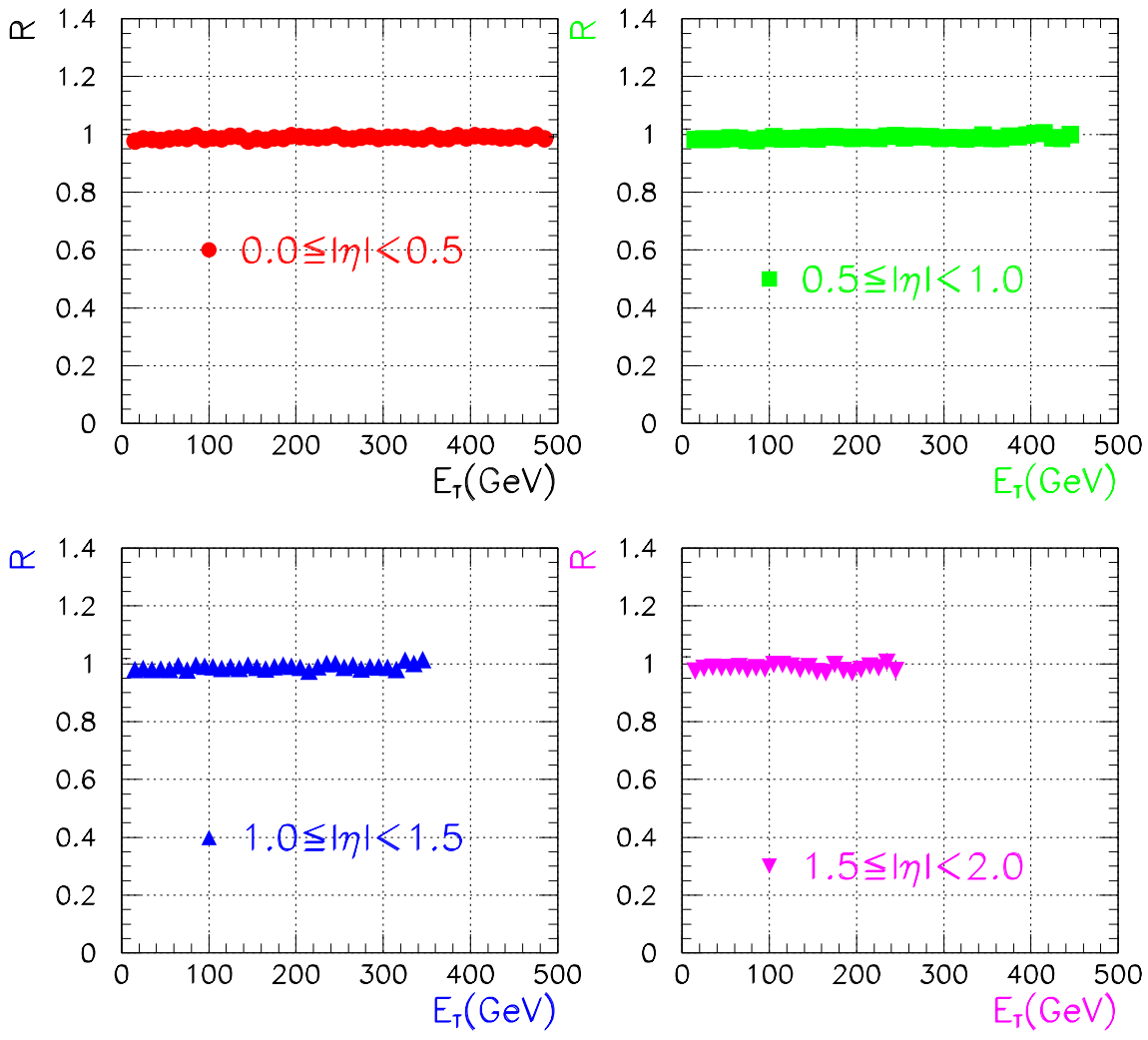

Figure 20: Ratio of R_{sep}=1.2/R_{sep}=1.3 cross sections for the four central $|\eta|$ slices.

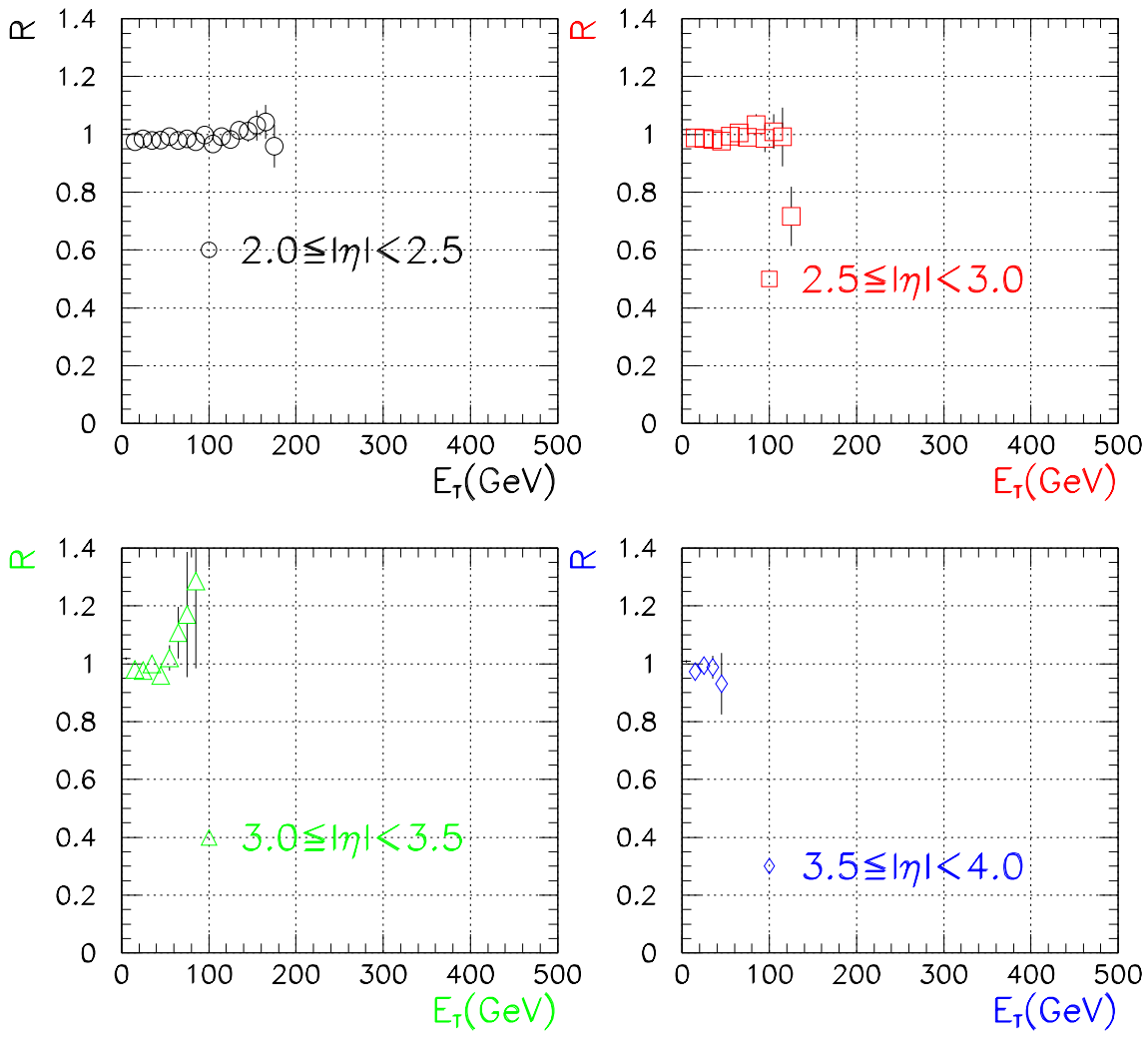

Figure 21: Ratio of R_{sep}=1.2/R_{sep}=1.3 cross sections for the four forward $|\eta|$ slices.

References

[1] S.D. Ellis, *priv. comm.*;

[2] J. Huth *et al.*, in proceedings of *Research Directions for the Decade, Snowmass 1990*, Editor E.L. Berger, (World Scientific, Singapore, 1992).

[3] F. Paige and S. Protopopescu, Report No. BNL38034, 1986 (unpublished).

[4] B. Abbott, Ph.D. Thesis, Purdue University (1994), unpublished; DØ collab., S. Abachi et al., *Phys. Lett.* **B357** (1995) 500.

[5] E.W.N. Glover, D.A. Kosower, private communication and Durham University preprint DTP/95/74. Los Alamos preprint: hep-ph/9510420.

[6] B. Abbott, Effects of η and ϕ Definitions on Reconstructing Jets, DØ internal note 2769.

[7] G. Marchesini and B.R. Webber,*Nucl. Phys.* **B310** (1988) 461, version 5.8.

[8] D. Elvira, G. Blazey, and R. Astur, A Study of Standard Jet Cuts and their Efficiencies Using DØ Collider Data, DØ internal note 1763.

[9] W.T. Giele, E.W.N. Glover and D.A. Kosower, *Nucl. Phys.* **B**403 (1993) 633.

[10] CTEQ Collab., J. Botts, et al., *Phys. Lett.* **B304** (1993) 159.

A Appendix: DØ jet definitions

The old way "DØ definition"	**The new way** Snowmass definition
during clustering use: η, ϕ a la Snowmass $\phi_{jet} = \frac{\sum_i E_T^i \phi^i}{\sum_i E_T^i}$; $\eta_{jet} = \frac{\sum_i E_T^i \eta^i}{\sum_i E_T^i}$	during clustering use: η, ϕ a la Snowmass $\phi_{jet} = \frac{\sum_i E_T^i \phi^i}{\sum_i E_T^i}$; $\eta_{jet} = \frac{\sum_i E_T^i \eta^i}{\sum_i E_T^i}$
measured quantities: $E_x = \sum_i E_x^i; E_y = \sum_i E_y^i; E_z = \sum_i E_z^i$ $E = \sum_i E^i$	measured quantities: $E_x = \sum_i E_x^i; E_y = \sum_i E_y^i; E_z = \sum_i E_z^i$ $E = \sum_i E^i$
$E_T = \sum_i E_T^i$	$E_T = \sum_i E_T^i$
$\theta_{jet} = \tan^{-1}(\frac{\sqrt{(\sum_i E_x^i)^2 + (\sum_i E_y^i)^2}}{\sum_i E_z^i})$	
$\phi_{jet} = \tan^{-1}(\frac{\sum_i E_y^i}{\sum_i E_x^i})$	$\phi_{jet} = \frac{\sum_i E_T^i \phi^i}{\sum_i E_T^i}$
$\eta_{jet} = -\ln(\tan(\theta_{jet}/2))$	$\eta_{jet} = \frac{\sum_i E_T^i \eta^i}{\sum_i E_T^i}$
internally **consistent** set of variables	**inconsistent** set of variables
given $E_T, \phi_{jet}, \eta_{jet}$ can calculate E_x, E_y, E_z and they **agree** with measured quantities $E_x = E_T \cos\phi_{jet}$ $E_y = E_T \sin\phi_{jet}$ $E_z = E_T \sinh\eta_{jet}$	given $E_T, \phi_{jet}, \eta_{jet}$ can calculate E_x, E_y, E_z and they **do not agree** with measured quantities $E_x \approx E_T \cos\phi_{jet}$ $E_y \approx E_T \sin\phi_{jet}$ $E_z \neq E_T \sinh\eta_{jet}$